

Measurement of the Neutron Magnetic Form Factor at High Q^2 Using the Ratio Method on Deuterium

G.P. Gilfoyle*, W.K. Brooks, and K. Hafidi *et al.* for the CLAS Collaboration

**E-mail: ggilfoyl@richmond.edu*

The 12-GeV Upgrade at Jefferson Lab will create an opportunity to dramatically extend our knowledge of the magnetic form factor of the neutron (G_M^n) and the other elastic, electromagnetic form factors. We describe here an approved experiment that will cover a Q^2 range ($3.5 - 14 \text{ GeV}^2$) with significant discovery potential. Different theoretical approaches (generalized parton distributions, Dyson-Schwinger equations, *etc*) diverge in this region and existing data cannot distinguish among them. The proposed measurement will be performed in Hall B with the CLAS12 detector and will have statistical and systematic uncertainties below 3%. It is based on the ratio of electron-neutron to electron-proton scattering that was successfully applied in the CLAS detector at Jefferson Lab.

Keywords: Form factors; Proceedings; World Scientific Publishing.

1. Introduction

The 12 GeV Upgrade at the Thomas Jefferson National Accelerator Facility (JLab) has begun and will double the beam energy and open new physics opportunities. The new physics program at JLab will dramatically extend the reach of our understanding of a fundamental feature of the neutron; its magnetic form factor G_M^n . The elastic electromagnetic form factors (EEFFs) describe the distribution of charge and magnetization inside the nucleon at low Q^2 and probe the quark structure at higher Q^2 . A broad program is planned at JLab to measure the EEFFs, map the internal landscape of the nucleon, and test non-perturbative Quantum Chromodynamics (QCD) and QCD-inspired models of the nucleon (see NSAC Long-Range Plan and others[1–7]). The measurement we discuss here will be performed with the new CLAS12 detector in Hall B (Experiment E12-07-104 [2]) at JLab which will replace the current and similar CLAS6 detector. CLAS12 is a large acceptance spectrometer consisting of layers of silicon counter, drift chambers, time-of-flight scintillators, electromagnetic calorimeters, and Čerenkov

counters. The forward part is based on a toroidal magnet and there is a central detector for particles emitted at large angles based on a solenoid magnet. The proposed measurement we describe here will cover the range $Q^2 = 3.5 - 14.0 \text{ GeV}^2$ with systematic uncertainties less than 3%. Statistical uncertainties will be about 3% in the highest Q^2 bin in this range and significantly less at lower Q^2 . The anticipated range and uncertainties of the experiment are shown in Figure 1. The reduced magnetic form factor $G_M^n/(\mu_n G_D)$ is plotted versus Q^2 where μ_n is the neutron magnetic moment and $G_D = 1/(1 + Q^2/\Lambda^2)^2$ is the dipole form factor with $\Lambda^2 = 0.71 \text{ GeV}^2$. We used the recent parameterization of the world's data on G_M^n in Ref [16] to predict the reduced form factor. Also shown are selected world's data for G_M^n including the recent CLAS6 results (red, open circles)[8]. The proposed CLAS12 experiment (black, closed squares) will nearly triple the upper limit of the previous CLAS6 measurement and provide precise data well beyond any existing measurement. In this paper we discuss the current experimental and theoretical situation and our method for measuring G_M^n with CLAS12.

2. Experimental Status

Figure 1 shows the world data for G_M^n up to $Q^2 = 14 \text{ GeV}^2$. For $Q^2 > 4.5 \text{ GeV}^2$ the data are sparse and have large uncertainties. In the range $Q^2 <$

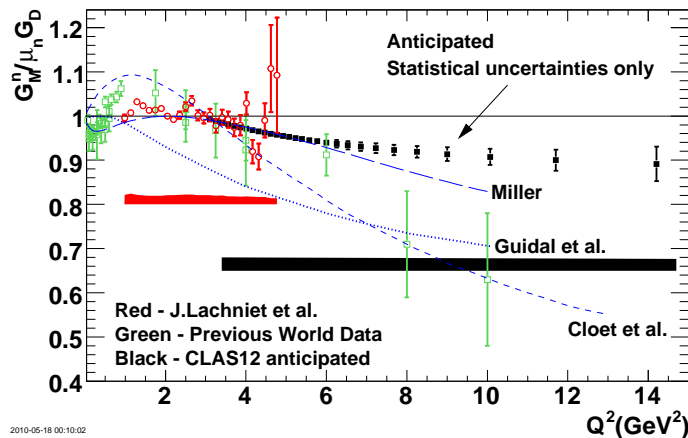


Fig. 1. Selected data [8–15] and anticipated results for G_M^n for 30 days of running with CLAS12 (black, filled squares) in units of $\mu_n G_D$ as a function of Q^2 . The anticipated CLAS12 results follow a fit to the world data on G_M^n that includes the CLAS6 G_M^n results [16] (red, open circles). Curves are described in the text.

4.5 GeV², the situation is much better especially with the addition of the CLAS6 measurement [8] (red, open circles). The CLAS6 measurement was performed using largely the same method we propose here for CLAS12. The CLAS6 data are surprisingly consistent with the dipole parameterization. This was unexpected because previous measurements show G_M^n decreasing at large Q^2 although with large uncertainties (green points in Figure 1 for $Q^2 \geq 4.5$ GeV²).

The broad effort at JLab to measure the EEFFS is in a Q^2 region with significant discovery potential. All these form factors are needed to untangle nucleon structure [17]. Measuring the ratio of the proton electric to magnetic form factor G_E^p/G_M^p using polarization observables revealed a striking dropoff contradicting previous measurements [18]. On the neutron side the ratio G_E^n/G_M^n was recently measured with greater precision and at higher Q^2 than ever before [19]. Those researchers used the recent CLAS6 measurement of G_M^n to extract G_E^n . The preliminary results for the points at Q^2 of 2.5 GeV² and 3.5 GeV² are 2-4 standard deviations away from the Galster parameterization; suggesting the onset of changes from the lower Q^2 behavior. All of these new, intriguing results are in the same Q^2 range as the proposed CLAS12 G_M^n measurement.

3. Theoretical Status

Progress has been made on the theory side of our understanding of the EEFFs. The interpretation of the form factors in relativistic kinematics has proven more challenging than expected and has required a new picture based on generalized parton distributions (GPDs) [20,21]. To understand non-perturbative QCD Cloët *et al.* employ a Dyson-Schwinger Equation approach and assume two of the valence quarks form a di-quark. Figure 2 shows the ratio of the neutron electric to magnetic form factors for two different values of the diquark radius (solid curve and long-dashed curve), data from Madey *et al.* [22], and the Kelly parameterization (dashed curve) [23]. The Cloët *et al.* prediction diverges dramatically from the data parameterization at $Q^2 \approx 5$ GeV² and crosses zero at $Q^2 \approx 11$ GeV². This behavior marks this region of Q^2 as one of potential discovery value and lies well within the Q^2 range of our proposed experiment. The prediction of G_M^n by Cloët *et al.* for G_M^n is shown in Figure 1 along with two other calculations. In Miller's calculation the nucleon is treated using light-front dynamics as a relativistic system of three bound quarks and a surrounding pion cloud [24]. The model gives a good description of much of the previous data (including the other three EEFFs) even at high Q^2 and is consistent

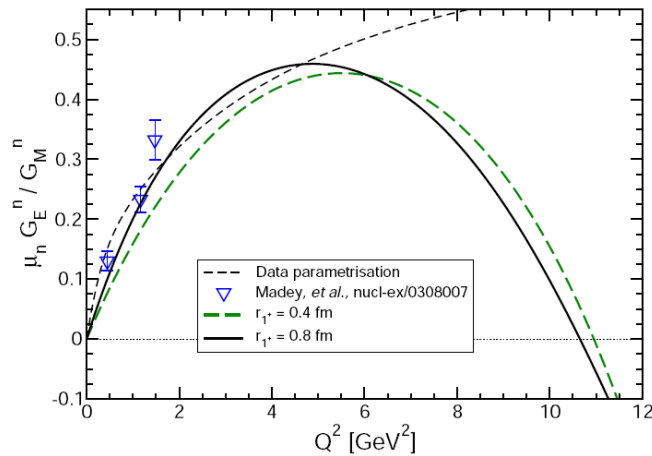


Fig. 2. Result for the normalized ratio of Sachs electric and magnetic form factors for the neutron computed with two different diquark radii. Short-dashed curve: parameterization of Ref. [23]. Down triangles: data from Ref. [22].

with the CLAS6 results. The curve from Guidal *et al* [25] uses GPDs to characterize the EEFs at low Q^2 and then extend their calculations to higher Q^2 , but fails to reproduce the data at low Q^2 . All three curves differ measurably in magnitude and/or slope in the range $Q^2 = 6 - 14 \text{ GeV}^2$. There is an opportunity here to distinguish among competing pictures.

We also want to touch on truly *ab initio* calculations performed using lattice QCD. These calculations are still limited in reach to $Q^2 \approx 1 \text{ GeV}^2$, but we expect that significant progress will be made by the time the proposed experiment is complete. This is where the broad assault on the EEFs at JLab is essential. The EEFs can be formed into isovector and isoscalar combinations that are sensitive to different physical effects. The isovector combination is free of disconnected contributions which are notoriously difficult to compute on the lattice. This freedom will make the isovector form factor an early test of lattice QCD as the calculations reach higher Q^2 .

4. Experimental Method

We now outline the experimental technique (more details are in Ref. [2]). We will use the ratio of quasielastic $e-n$ to $e-p$ scattering from a deuterium target to measure G_M^n . This technique reduces uncertainties associated with other methods and has been used by us [8] and others [12,26–29] (see Figure

1). The method is based on the ratio

$$R = \frac{\frac{d\sigma}{d\Omega}(^2\text{H}(e, e'n)_{QE})}{\frac{d\sigma}{d\Omega}(^2\text{H}(e, e'p)_{QE})} = a(Q^2) \frac{\sigma_{mott}^n (G_E^{n2} + \frac{\tau_n}{\epsilon_n} G_M^{n2}) \left(\frac{1}{1+\tau_n}\right)}{\frac{d\sigma}{d\Omega}(^1\text{H}(e, e')p)} \quad (1)$$

for quasielastic (QE) kinematics. The right-hand side is written in terms of the free nucleon form factors and where $\tau = Q^2/4M^2$ and $\epsilon = 1/[1 + 2(1 + \tau) \tan^2(\theta/2)]$. Deviations from this ‘free ratio’ assumption are parameterized by the factor $a(Q^2)$ which can be calculated from deuteron models and is close to unity at large Q^2 . The results of other measurements of the proton cross section and the neutron electric form factor are used to extract G_M^n . The ratio R is insensitive to the luminosity, electron acceptance, electron reconstruction efficiency, trigger efficiency, the deuteron wave function used in $a(Q^2)$, and radiative corrections [8].

We will first select quasielastic (QE) events by applying a cut on θ_{pq} , the angle between the nucleon 3-momentum and the momentum transfer \vec{q} . Nucleons from inelastic events nucleons tend to be emitted at large θ_{pq} while QE nucleons are emitted along \vec{q} . Analyzing protons and neutrons the same way avoids biasing the results. Next, we select events with $W^2 = M_N^2$, but at high Q^2 the width of the residual mass spectrum W^2 and contaminates the QE peak. The top panel of Figure 3 shows the results of a simulation for such high- Q^2 $e - n$ events. The red histogram shows the QE events, the green one shows the inelastic events, and the black one is the total. The QE events are overwhelmed by the inelastic background. Requiring $\theta_{pq} < 1.5^\circ$ for the neutron (lower-left-hand panel) considerably reduces the inelastic background, but the QE events are still a shoulder on a larger inelastic peak. We now take advantage of the large acceptance of CLAS12. The inelastic events emit additional particles (pions, photons, *etc.*) and CLAS12 will detect many of those particles. In the lower-right-hand panel we have applied a hermiticity cut; rejecting events with a third particle. The quasielastic peak now clearly rises out of the inelastic noise. We emphasize here that Figure 3 is a worst case scenario. We simulated the reaction for the highest Q^2 bin (12.5 – 14 GeV²) where the inelastic contamination is largest. The data at lower Q^2 will have less kinematic spreading and inelastic contamination.

The CLAS12 G_M^n measurement has important consistency checks. Neutrons will be measured in two subsystems of CLAS12: the forward electromagnetic calorimeter (FC) and the forward time-of-flight (TOF). These two subsystems will enable us to make semi-independent measurements of the $e - n$ production and provide a cross check. The CLAS12 measurement will

also have a large overlap ($Q^2 = 3.5 - 4.8 \text{ GeV}^2$) with the previous CLAS6 G_M^n one (see Figure 1).

An essential aspect of the neutron measurement in the TOF and FC systems is measuring the neutron detection efficiency. We will use the $p(e, e' \pi^+ n)$ reaction as a source of tagged neutrons. Electrons and π^+ 's will be detected in CLAS12 and missing mass used to select candidate neutrons (found events). We then predict the position of the neutron in CLAS12 and search for it (if a neutron is observed we call these reconstructed events). The ratio of reconstructed to found events is the detection efficiency. This will be done in CLAS12 with a unique, dual target. Co-linear, liquid hydrogen and deuterium cells will provide production and calibration events simultaneously and under the same conditions (*in situ*). This reduces our vulnerability to variations in detector gains, beam properties, *etc.* In the

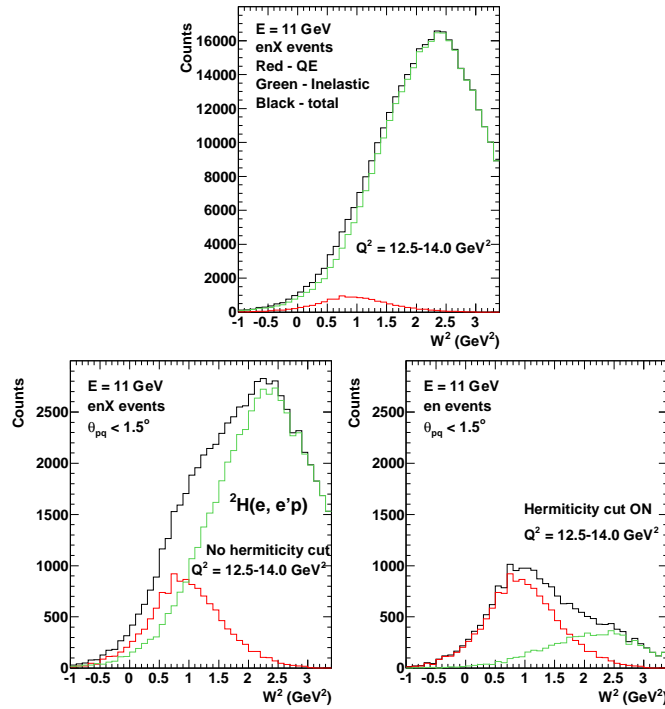


Fig. 3. The impact of the hermiticity cut is shown. The top panel displays the W^2 spectra for simulated $e-n$ events. In the lower-left-hand panel, the neutrons are required to have $\theta_{pq} < 1.5^\circ$. In the lower-right-hand panel, we add the hermiticity cut. The number of events shown is not representative of the anticipated value.

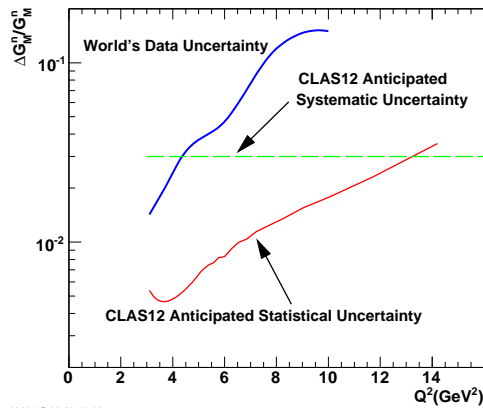


Fig. 4. Run statistics for the CLAS12 G_M^n experiment (E12-07-104) for 30 days of running. The blue, solid curve is the current uncertainty on G_M^n for the world data, the green, dashed line is our anticipated statistical uncertainty, and the red, solid curve is our goal of 3% systematic uncertainty.

CLAS6 measurement we used the same techniques and found the different data sets were consistent within the statistical uncertainties [8].

In Figure 4 we show the anticipated uncertainty on G_M^n (red, solid line). Proton cross sections came from Ref [23] and neutron cross sections from Galster (G_E^n) and Alberico *et al.* (G_M^n) [16]. We included the effect of a cut requiring $W^2 < 1.2 \text{ GeV}^2$ that reduces residual inelastic contamination. Over the range $Q^2 = 3.5 - 14.0 \text{ GeV}^2$ we have statistical uncertainties at or below 3% (green, dashed line) and typically much lower. These uncertainties are far better than the current precision on G_M^n (blue, solid line).

5. Summary

To summarize, the scientific motivation for measuring the neutron magnetic form factor is compelling. At higher Q^2 ($5 - 13 \text{ GeV}^2$) we have observed new, surprising behavior in the other form factors and developed QCD-inspired models that diverge widely. To explore this new territory JLab will measure all of the EEFs. The CLAS12 experiment will use a tested method for measuring G_M^n and push the frontier of our understanding of the neutron magnetic form factor up to $Q^2 = 14 \text{ GeV}^2$ and with high precision. The ability to veto multiparticle final states dramatically reduces the background from inelastic events that contaminate the QE peak. We will use a dual-cell target for precise, *in situ* measurements of the neutron

detection efficiency as demonstrated in the CLAS6 experiment. Finally, with CLAS12 we have several important consistency checks using different detector subsystems of CLAS12 (TOF and EC) to validate our results.

References

1. Nuclear Science Advisory Committee, *The Frontiers of Nuclear Science* (US Department of Energy, 2007).
2. G. Gilfoyle *et al.*, Experiment E12-07-104, Jefferson Lab (Newport News, VA, 2007).
3. E. Brash *et al.*, Experiment E12-09-001, Jefferson Lab (Newport News, VA, 2009).
4. S. Gilad *et al.*, Experiment E12-07-108, Jefferson Lab (Newport News, VA, 2007).
5. B. Quinn *et al.*, Experiment E12-09-119, Jefferson Lab (Newport News, VA, 2009).
6. B. Anderson *et al.*, Experiment E12-09-006, Jefferson Lab (Newport News, VA, 2009).
7. B. Wojtsekhowski *et al.*, Experiment E12-10-005, Jefferson Lab (Newport News, VA, 2010).
8. J. Lachniet, A. Afanasev, H. Arenhövel, W. K. Brooks, G. P. Gilfoyle, D. Higginbotham, S. Jeschonnek, B. Quinn, M. F. Vineyard *et al.*, *Phys. Rev. Lett.* **102**, p. 192001 (2009).
9. W. Bartel *et al.*, *Nucl. Phys. B* **58**, p. 429 (1973).
10. G. Kubon *et al.*, *Phys. Lett. B* **524**, 26 (2002).
11. A. Lung *et al.*, *Phys. Rev. Lett.* **70**, 718(Feb 1993).
12. H. Anklin *et al.*, *Phys. Lett. B* **428**, 248 (1998).
13. B. Anderson *et al.*, *Phys. Rev. C* **75**, p. 034003 (2007).
14. R. G. Arnold *et al.*, *Phys. Rev. Lett.* **61**, 806(Aug 1988).
15. S. Rock *et al.*, *Phys. Rev. Lett.* **49**, 1139(Oct 1982).
16. W. M. Alberico, S. M. Bilenky, C. Giunti and K. M. Graczyk, *Phys. Rev. C (Nuclear Physics)* **79**, p. 065204 (2009).
17. M. Diehl, T. Feldmann, R. Jakob and P. Kroll, *Eur. Phys. J. C* **39**, p. 1 (2005).
18. M. K. Jones *et al.*, *Phys. Rev. Lett.* **84**, 1398(Feb 2000).
19. K. de Jager (2009).
20. G. A. Miller, *Phys. Rev. Lett.* **99**, p. 112001 (2007).
21. G. A. Miller and J. Arrington, *Phys. Rev. C* **78**, p. 032201 (2008).
22. R. Madey *et al.*, *Phys. Rev. Lett.* **91**, p. 122002 (2003).
23. J. J. Kelly, *Phys. Rev. C* **70**, p. 068202(Dec 2004).
24. G. Miller, *Phys. Rev. C* **66**, p. 032201 (2002).
25. M. Guidal *et al.*, *Phys. Rev. D* **72**, p. 054013 (2005).
26. C. Hyde-Wright and K.deJager, *Ann. Rev. Nucl. Part. Sci.* **54**.
27. H. Anklin *et al.*, *Phys. Lett. B* **336**, 313 (1994).
28. G. Kubon *et al.*, *Phys. Lett. B* **524**, 26 (2002).
29. E. E. W. Bruins *et al.*, *Phys. Rev. Lett.* **75**, 21(Jul 1995).